Correlation of Alfvén wave Poynting flux in the plasma sheet at 4–7 R_E with ionospheric electron energy flux

A. Keiling,[1] J. R. Wygant,[1] C. Cattell,[1] W. Peria,[2] G. Parks,[2] M. Temerin,[3] F. S. Mozer,[3] C. T. Russell,[4] and C. A. Kletzing[5]

Received 4 April 2001; revised 10 September 2001; accepted 10 September 2001; published 25 July 2002.

[1] A comparison of Poynting flux in the plasma sheet at geocentric distances of 4–7 R_E to the energy flux of magnetically conjugate precipitating electrons at 100-km altitude is presented. We have investigated 40 plasma sheet crossings by the Polar satellite, including both cases with large in situ values of Poynting flux (~1 ergs cm^{-2} s^{-1}) and cases with low values (≤0.1 ergs cm^{-2} s^{-1}). The values correspond to ~125 and ~12 ergs cm^{-2} s^{-1}, respectively, when mapped along converging magnetic field lines to 100 km. The north-south component of the electric field and the east-west component of the magnetic field were the primary source of the Poynting flux. On the basis of the phase relationship and ratio of **E** and **B**, the majority of Poynting flux events were identified as Alfvén waves. The Poynting flux measured at high altitudes by Polar was correlated with the intensity of the conjugate auroral emission in the ultraviolet frequency range, which can be used to estimate energy deposition due to precipitating electron beams. The electron energy flux during times of intense Poynting flux in the plasma sheet exceeded 20 ergs cm^{-2} s^{-1}. In the absence of strong Poynting flux in the plasma sheet, electron precipitation was small (≤5 ergs cm^{-2} s^{-1}). The mapped Poynting flux was in almost all events larger by a factor of 1–10 than the ionospheric electron energy flux. These results show that Alfvénic Poynting flux in the midtail region is associated with and capable of powering localized regions of magnetically conjugate auroral emissions. Furthermore, the large Poynting flux events observed at the outer edge of the plasma sheet were conjugate to the poleward border of the active auroral regions, giving further evidence that at least some of the discrete aurora connects to the plasma sheet boundary layer. *INDEX TERMS:* 2704 Magnetospheric Physics: Auroral phenomena (2407); 2716 Magnetospheric Physics: Energetic particles, precipitating; 2736 Magnetospheric Physics: Magnetosphere/ionosphere interactions; *KEYWORDS:* Alfven wave, auroral phenomena, Poynting flux, plasma sheet, substorm, magnetospheric-ionospheric interaction

1. Introduction

[2] Recent studies using the Polar satellite show that very large amplitude electric fields ($E_\perp$ > 100 mV m^{-1}) are often observed in the plasma sheet boundary layer (PSBL) at geocentric distances of 4–7 R_E [*Wygant et al.*, 2000; *Keiling et al.*, 2001]. It was shown that the dominant electric field component is perpendicular to the nominal plasma sheet. Previous studies of electric fields, using ISEE 1/2 [*Mozer*, 1981; *Cattell et al.*, 1982] and Geotail [*Cattell et al.*, 1994; *Streed et al.*, 2001], provided evidence for large-amplitude spiky electric fields at geocentric distances from 4 to 100 R_E, but the measurements were restricted to the components that lie in the ecliptic plane. In a statistical study using 2 years of Polar electric field data ($E_\perp$), *Keiling et al.* [2001] showed that these fields delineate the statistical auroral oval similar to the low-altitude (~1 R_E) electric field distribution observed by S3-3 [*Bennett et al.*, 1983], indicating the relevance of high-altitude electric fields to auroral processes. It was also shown in the Polar study that the fields do not only map like quasi-static electric fields, as shown by previous studies [*Mozer*, 1981; *Levin et al.*, 1983], but are also consistent with the propagation of Alfvén waves along converging magnetic field lines. *Wygant et al.* [2000] showed for two Polar case studies that the perpendicular electric fields in the PSBL at 4–6 R_E were associated with Alfvén waves, which carried large and sufficient Poynting flux toward the ionosphere to power magnetically conjugate auroral emissions. *Keiling et al.* [2000] have shown that large Alfvénic Poynting flux often occurs in the PSBL during the expansion phase of substorms. These

[1]School of Physics and Astronomy, University of Minnesota, Minneapolis, Minnesota, USA.
[2]Geophysics Program, University of Washington, Seattle, Washington, USA.
[3]Space Sciences Laboratory, University of California, Berkeley, California, USA.
[4]Institute of Geophysics and Planetary Physics, University of California, Los Angeles, California, USA.
[5]Department of Physics and Astronomy, University of Iowa, Iowa City, Iowa, USA.

0148-0227/02/2001JA900140$09.00

recent Polar observations have clearly demonstrated the connection between auroral phenomena and energy transfer processes by large Alfvén waves in the PSBL. *Maynard et al.* [1996], *Keiling et al.* [2001], and *Toivanen et al.* [2001] also showed that large Poynting flux occurs in the central plasma sheet during times of auroral substorms.

[3] In this paper we continue to investigate the coupling between the plasma sheet and the ionosphere via Poynting flux measured in the region between the distant magnetotail and the auroral acceleration region. In addition to in situ measurements, Polar simultaneously takes images of auroral emissions in the ionosphere using the Ultraviolet Imager (UVI). These images can be used to estimate energy depositions by electron beams into the ionosphere. Tracing Polar's location along magnetic field lines to its ionospheric foot point allows a direct comparison of two different, magnetically conjugate regions from an energetic point of view. We have investigated 40 plasma sheet crossings, some of which had large values ($\sim$1 ergs cm^{-2} s^{-1}) and some of which had low values ($\leq$0.1 ergs cm^{-2} s^{-1}) of Poynting flux, and compared them to low-altitude energy deposition due to electrons. The primary result of this study is that there is a good correlation of intensity between Poynting flux at 4–7 R_E and ionospheric electron energy flux. The majority of the Poynting flux events were due to Alfvén waves. Hence we provide further evidence that intense, localized electromagnetic energy flux, dominated by Alfvén waves, at 4–7 R_E is an important energy source for auroral arc formation (auroral emissions). In addition, we address the issue of mapping auroral arcs to the magnetosphere. The PSBL is identified as a region that maps to the poleward border of auroral regions.

[4] The occurrence of auroral arcs during the growth phase, expansion phase, and recovery phase is a fundamental ionospheric signature of magnetospheric substorms. It has long been known [e.g., *McIlwain*, 1960] that auroral arcs are generated through the impact of accelerated energetic electron beams with ionospheric molecules and atoms. Soon after the discovery of large perpendicular electric fields at altitudes between 1000 and 8000 km using S3-3 data [*Mozer et al.*, 1977], it was found that large perpendicular electric fields (called electrostatic shocks by early researchers) below and in the auroral acceleration region are associated with auroral arcs [*Torbert and Mozer*, 1978; *Kletzing et al.*, 1983]. Some low-altitude fields ($\sim$1700 km) have later been identified as kinetic Alfvén waves [*Louarn et al.*, 1994; *Wahlund et al.*, 1994]. Theoretical works suggest that kinetic Alfvén waves could provide the necessary energy and a mechanism to transfer the wave energy to particle energy [*Hasegawa*, 1976; *Goertz*, 1984].

[5] t is generally accepted that the energy necessary to cause auroral emissions is provided by the magnetotail, although the exact sequence of energy transfer processes from crossing the magnetopause to the acceleration of auroral electrons is still unknown. During substorms the magnetotail releases large amounts of its stored magnetic energy. Besides the downtail release of plasmoids, some of the energy is dissipated through auroral emissions, Joule heating in the ionosphere, and ring current enhancement. The work presented here focuses on the identification of the magnetospheric energy carriers leading to the auroral arc generation. Theoretical and observational results offer a variety of scenarios for the conversion and transfer of stored magnetic energy in the magnetotail to ultimately the kinetic energy of auroral electrons. Reconnection processes in the tail have been invoked, which could convert magnetic energy of a stretched magnetotail into field-aligned particle beams and bulk plasma flows [*Baker et al.*, 1996, and references therein]. Bursty bulk flow (BBF) has been investigated in association with the transport of energy from the distant tail to the near-tail region using Geotail data [*Angelopoulos et al.*, 1992]. Investigations of flow bursts at 10–15 R_E in the premidnight equatorial magnetotail demonstrated that such events were closely associated with auroral brightenings [*Fairfield et al.*, 1999]. Reconnection processes or BBF might also be the source of Alfvén waves in the PSBL above the auroral acceleration region, reported by *Wygant et al.* [2000] and *Keiling et al.* [2000], which then carry electromagnetic energy toward the ionosphere. The earliest reports for the importance of Alfvén waves for energy transport in the auroral ionosphere and magnetosphere came from ground-based observations in the auroral zone. The ground-based observations give indications of strong ULF (1–10 mHz) Alfvén wave activity at both boundaries of the auroral region. Alfvén field-aligned resonances are seen in association with auroral arcs near the equatorial border of the auroral regions [*Samson et al.*, 1991, 1996; *Liu et al.*, 1995].

2. Data Analysis

[6] The Polar satellite has an 18-hour polar orbit (originally 80° inclination), with perigee and apogee of 2.2 and 9 R_E (geocentric distance), respectively. Hence it offers the opportunity to examine the plasma sheet and its poleward boundary at geocentric distances of 4–7 R_E. This region stands intermediate between the auroral acceleration region at 1–3 R_E and the more distant portions of the magnetotail. A study of this region can be of relevance for processes in the auroral acceleration region and in the magnetotail. In addition, the Polar spacecraft is the first spacecraft that allows high-resolution three-dimensional (3-D) measurements of the electric field in this region.

[7] The Polar satellite is equipped with a number of instruments. For this study we incorporated data from the University of California (UC) Berkeley Electric Field Instrument [*Harvey et al.*, 1995], the UCLA fluxgate magnetometer [*Russell et al.*, 1995], the University of Washington Ultraviolet Imager [*Torr et al.*, 1995], and the University of Iowa Hydra Plasma Instrument [*Scudder et al.*, 1995]. The electric field is determined from a measurement of the electric potential difference between pairs of current-biased spherical sensors, deployed at the ends of three orthogonal pairs of booms with tip-to-tip separations of 100 and 130 m (in the spin plane) and 28 m (along the spin axis). The three-axis electric field vector is sampled at 20 samples s^{-1}. The magnetic field vector is sampled at $\sim$8.3 samples s^{-1} by the UCLA 3-D fluxgate magnetometer. Hydra measurements of electron and ion energy flux at 13.8-s time resolution in the energy range from 12 eV to 18 keV were used.

[8] Electric and magnetic field measurements were used to calculate magnetic field-aligned Poynting fluxes, $S_{\parallel}$, at the satellite location:

$$S_{\parallel} = \vec{S} \cdot \frac{\vec{B}}{|\vec{B}|}, \quad (1)$$

where $\vec{B}$ is the local magnetic field and $\vec{S}$ is the Poynting vector. The relevant fields that were used to calculate the Poynting flux are the perturbation electric ($\delta\vec{E}$) and magnetic ($\delta\vec{B}$) fields:

$$\vec{S} = \frac{1}{\mu_0} \delta\vec{E} \times \delta\vec{B}. \quad (2)$$

[9] Strictly speaking, it is only the integral over a volume of the Poynting flux that is physically significant [*Kelley et al.*, 1991]. For space physics applications this is most often impractical because regions of mere energy flow and regions of energy dissipation can be separated by very large distances, and simultaneous measurements of electric and magnetic fields in the different regions are not available. However, physical insight into the problem may allow one to reason for its relevance.

[10] In the context of this paper the measured magnetic field is $\vec{B} = \vec{B}_0 + \delta\vec{B}$, where $\vec{B}_0$ is the background magnetic field and $\delta\vec{B}$ is a perturbation field. Two sources of electric and magnetic perturbation fields can be identified here: Alfvén waves and quasi-static electric fields associated with field-aligned currents (FACs) that close in the ionosphere or at altitudes below the satellite. Both sources have magnetic and electric field perturbations with the same polarization and are associated with Poynting flux propagating along magnetic field lines.

[11] There are two contributions to the Poynting flux associated with Alfvén waves. One contribution represents the convective transport of flux perpendicular to the background magnetic field and is proportional to $\delta\vec{E} \times \vec{B}_0$. This contribution is zero when averaged over many wave periods. The contribution that accounts for the transport of energy along the background magnetic field is entirely due to the perturbation electric ($\delta\vec{E}$) and magnetic ($\delta\vec{B}$) fields and is given by (2). This is the component of interest for this study. In the case of static fields the situation is similar. Only $\delta\vec{E}$ and $\delta\vec{B}$ contribute to the physically meaningful Poynting flux. As shown by *Kelley et al.* [1991], the quantity $\delta\vec{E} \times \vec{B}_0$ does not contain any useful information concerning energy flow or dissipation.

[12] Throughout this paper, values of Poynting flux are either given as in situ values or given as extrapolated values into the ionosphere. The latter is calculated by assuming that both Alfvén waves and static fields carry Poynting flux along magnetic field lines to ionospheric altitudes (100 km). In the absence of energy conversion and perpendicular Poynting flux, the Poynting flux at different altitudes scales proportionally with the background magnetic field strength:

$$S_I = S_H \cdot \frac{B_I}{B_H}, \quad (3)$$

where S and B are the Poynting flux and the background magnetic field, respectively. The indices I and H indicate the ionospheric and high-altitude values, respectively. The ratio B_I/B_H was calculated for each event, based on the measured in situ magnetic field strength and a fixed value of 50,000 nT for the ionosphere.

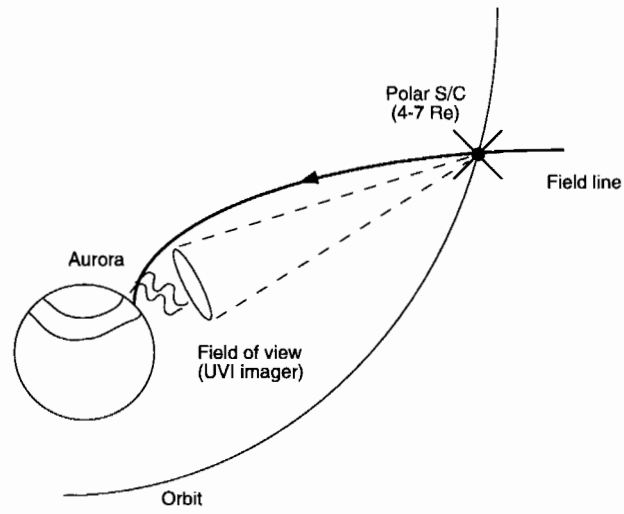

Figure 1. Experimental setup.

[13] The Poynting fluxes at high altitude were compared to magnetically conjugate, ionospheric electron energy flux. This was achieved by tracing Polar's location along magnetic field lines, using the International Geomagnetic Reference Field (IGRF), into the ionosphere (~100 km) and using simultaneous ultraviolet images (UVI) of the aurora (Figure 1). In addition to information on the spatial location of auroras, estimates of energy flux of auroral electrons depositing energy into the ionosphere can be inferred from the images [*Torr et al.*, 1995]. The UVI instrument utilizes four different filters to provide spectral information on the aurora. In this study, images were obtained using a filter centered on 1700 Å with a band width of ~80 Å. This filter responds to molecular N_2 Lyman-Birge-Hopfield (LBH)-long wavelength emissions, which are primarily due to electron impact excitation. The intensity of auroral emissions at this wavelength is approximately proportional to the total energy flux deposited by auroral electrons in the ionosphere. Its accuracy is estimated to be ~50% [*Germany et al.*, 1998].

3. Case Studies

[14] In this section we present comparisons between the Poynting flux measured at high altitude and energy deposition by electron beams into the ionosphere on the same field line during two Polar plasma sheet passes. For the first event, Polar was magnetically conjugate to intense aurora. For the second event, Polar was magnetically conjugate to weak aurora.

3.1. Plasma Sheet Crossing on 21 April 1997

[15] During the plasma sheet crossing on 21 April 1997, Polar encountered strong Poynting fluxes in the PSBL that were magnetically conjugate to intense auroral emissions. The entire crossing of the plasma sheet took ~70 min. This time period coincided with a substorm.

[16] Figure 2 shows ultraviolet images of auroral emissions together with Polar in situ field and particle data. The

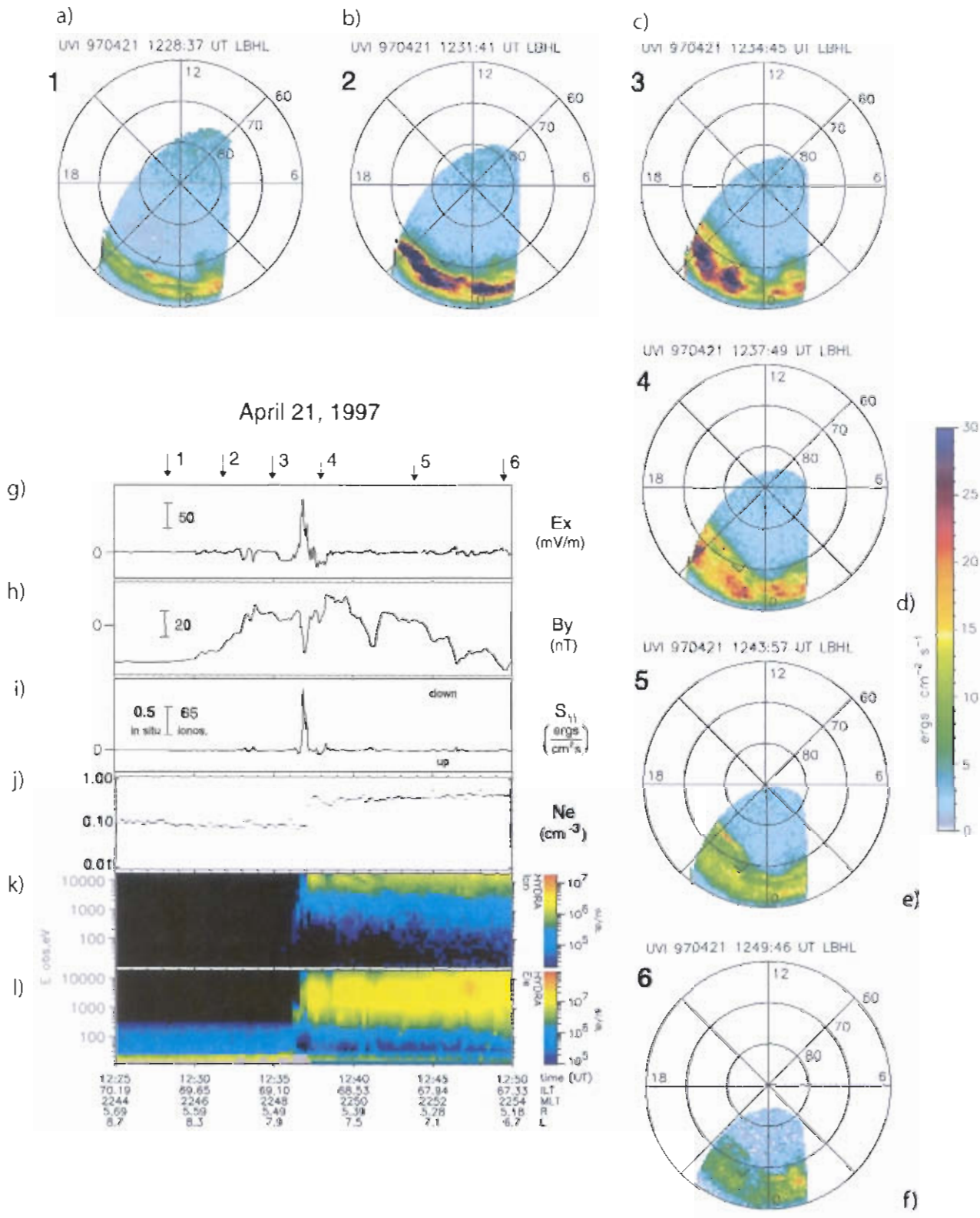

Figure 2. (a–l) Measurements from the Polar satellite on 21 April 1997 during a plasma sheet crossing. Figures 2a–2f show images of the aurora from the Ultraviolet Imager (UVI) instrument on board Polar during the same plasma sheet crossing shown. These images also provide an indicator of the total energy deposited in the ionosphere by electrons (color scale). Small arrows indicate the track of the satellite. Figures 2g–2l show one electric field component (6-s averaged) approximately normal to the plane of the plasma sheet, the east-west component of the magnetic field (model subtracted), the Poynting flux component along the magnetic field (see text for calculation method), the electron density, and energy-time spectrograms of ions and electrons, respectively.

electric and magnetic field data are averaged over 6 s. Figure 2g shows the E_x component of the electric field in a magnetic field-aligned coordinate system. This component is approximately normal to the nominal plasma sheet. Figure 2h shows the B_y component of the magnetic field after subtracting a model field. This component is directed perpendicular (east-west) to the Earth's magnetic field and lies approximately in the plane of the plasma sheet. Figure 2i shows the parallel Poynting flux calculated from the three components of the perturbation electric field and the three components of the perturbation magnetic field, calculated by detrending each component by subtracting a 3-min running average from the original data (detrended individual components are not shown). The Poynting flux vector was then projected onto the average magnetic field direction, calculated by averaging the magnetic field vector over 3 min. Note that the detrending of the components, E_x and B_y, removes any Poynting flux due to large-scale, field-aligned currents. Figure 2j shows electron density, obtained by integrating the electron distribution measured by Hydra. Figures 2k and 2l show the energy spectra of ions and electrons, respectively.

[17] The 21 April 1997 lobe-PSBL crossing is characterized by the sharp flux increase of ions and electrons at 1236 UT seen in Figures 2k and 2l, which coincides with a steep density increase from 0.1 to 0.4 cm^{-3} (Figure 2j). Immediately following the entry, Polar encountered large electric and magnetic field perturbations. The magnetic field perturbation due to Alfvén waves was superimposed on large-scale changes due to field-aligned currents. The perturbation fields near the lobe-PSBL interface were very similar in waveform with peak amplitudes of -130 mV m^{-1} and -14 nT. The field-aligned Poynting flux associated with these smaller-scale fluctuations (Figure 2i) was directed downward toward the ionosphere and was largest near the lobe-PSBL interface ($\sim$1 ergs cm^{-2} s^{-1}). If this Poynting flux reached an altitude of 100 km, it would be increased to $\sim$125 ergs cm^{-2} s^{-1}. Section 2 describes the calculation for this mapping. The ratio of the peak electric to magnetic field perturbation is $\sim$9300 km s^{-1}. This is comparable to the local Alfvén speed of $\sim$11,000 km s^{-1} determined from in situ plasma parameters. The correlated electric and magnetic field perturbations are thus consistent with the propagation of Alfvén waves along the magnetic field. We point out that the Poynting flux associated with large-scale, field-aligned currents was much smaller for this event. This was generally true for all intense, localized Poynting flux events investigated in this paper (see section 4). A comparison of the different contributions is explicitly shown for one Polar event by [*Wygant et al.*, 2002].

[18] The six UV images in Figure 2 show the spatio-temporal evolution of the aurora. Small arrows indicate the mapped foot of the Polar magnetic field line at the times the UVI images were taken and the direction of Polar's trajectory. These times are also indicated by arrows above Figure 2g. The estimated accuracy of the mapping is $\sim$1°. The color scale next to the images gives the estimated electron energy flux causing the auroral emission in units of ergs cm^{-2} s^{-1}. Figure 2a shows two arc systems at the equatorward edge ($\sim$62°) and the poleward edge ($\sim$68°) of the auroral oval between 2100 and 0100 magnetic local time (MLT). Polar's foot point is in the polar cap region at the time when this image was taken. By the time the next image (Figure 2b) was taken, both arc systems had brightened. The equatorward arc system had also expanded poleward. Both arc systems can still be vaguely discerned. According to the *AE* index, at $\sim$1230 UT a strong intensification ($\sim$500 nT) occurred, i.e., between the times of Figures 2a and 2b. At this time, Polar was still in the tail lobe. However, coinciding with the intensification, Polar recorded the magnetic effect of a strong FAC with smaller magnetic field perturbations superimposed and with electric field perturbations in the Pi2 frequency range. In Figure 2c the two initial arc systems had joined, and the poleward edge had further expanded. Polar's foot point maps to the poleward edge of the very intense aurora ($\geq$20 ergs cm^{-2} s^{-1}). Allowing for the mapping uncertainty, it is possible that Polar's field line actually entered this very active region between Figures 2c and 2d. This time interval coincides with the occurrence of large in situ Poynting flux, which lasted for $\sim$1 min in the spacecraft frame. In comparison, the peak electron energy flux conjugate to the satellite position is $\sim$25 ergs cm^{-2} s^{-1}. Note that this value might be underestimated because the UVI intensity is averaged over one entire pixel. Hence individual arcs that cannot be resolved might be more intense. This energy balance, nevertheless, makes it feasible for the high-altitude Poynting flux to indeed be responsible for providing the energy for the energetic electron flux. This is also supported by the fact that the Poynting flux shows only very little reflected power, implying that it must be dissipated at lower altitudes. The difference in energy flux of 100 ergs cm^{-2} s^{-1} can also account for other processes such as ion acceleration, Joule heating in the ionosphere, spatial broadening of Poynting flux, and electron beams below the satellite location [*Wygant et al.*, 2000, and references therein]. Figure 2d shows much reduced auroral emission. We thus conclude that it is very likely that the intense auroral region was magnetically conjugate to intense Poynting flux at Polar's altitude. This interpretation is consistent with many other events included in the statistical part of this paper (section 4).

[19] Later images (Figures 2e and 2f) show that the intensity of the aurora reduced rapidly. Figures 2e and 2f show two arc systems (equatorward and poleward), which are a common auroral substorm recovery signature [*Elphinstone et al.*, 1993]. The only interval with strong Poynting fluxes during the entire plasma sheet crossing was at the outer edge of the plasma sheet. Because of the extreme angle of the UVI camera with regard to the auroral oval, the imager is routinely turned off at lower latitude, so that no images were available after 1250 UT.

[20] Ground magnetometer data for this event were presented by *Keiling et al.* [2000], showing a 500-nT negative bay at Tixie. It was shown that the strong Poynting flux occurred during the expansion phase. Thus this example clearly shows the connection of auroral phenomena, such as auroral brightening, negative H bay, and electromagnetic energy flow in the PSBL.

3.2. Plasma Sheet Crossing on 6 April 1997

[21] In contrast to the event on 21 April 1997, this plasma sheet pass occurred when the aurora was much

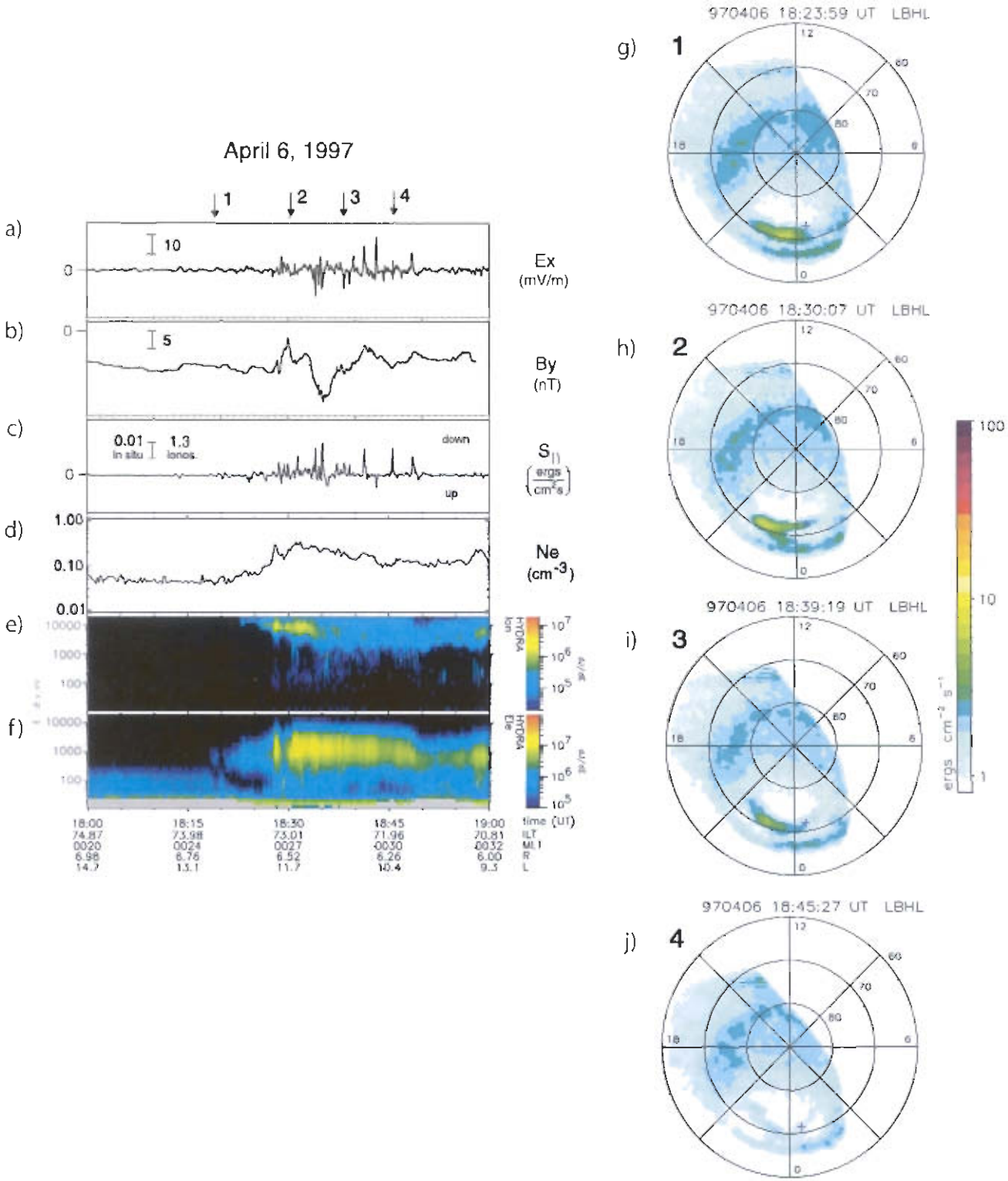

Figure 3. (a–j) Measurements from the Polar satellite on 6 April 1997 during a plasma sheet crossing. The format is the same as that in Figure 2.

quieter (Kp = 1, AE = 30 nT), resulting in a number of differences in the plasma sheet signature as well as in the auroral emission. Figure 3 shows the inbound pass on 6 April 1997 by Polar. The panels are in the same format as those in Figure 2. The satellite entered the plasma sheet from the lobe at ~1825 UT at an altitude of ~6.5 R_E and an L value of ~12. The larger L value indicates that the plasma sheet was expanded. Along with this goes a much more

Poynting flux events larger than 10 ergs $cm^{-2} s^{-1}$ (mapped)

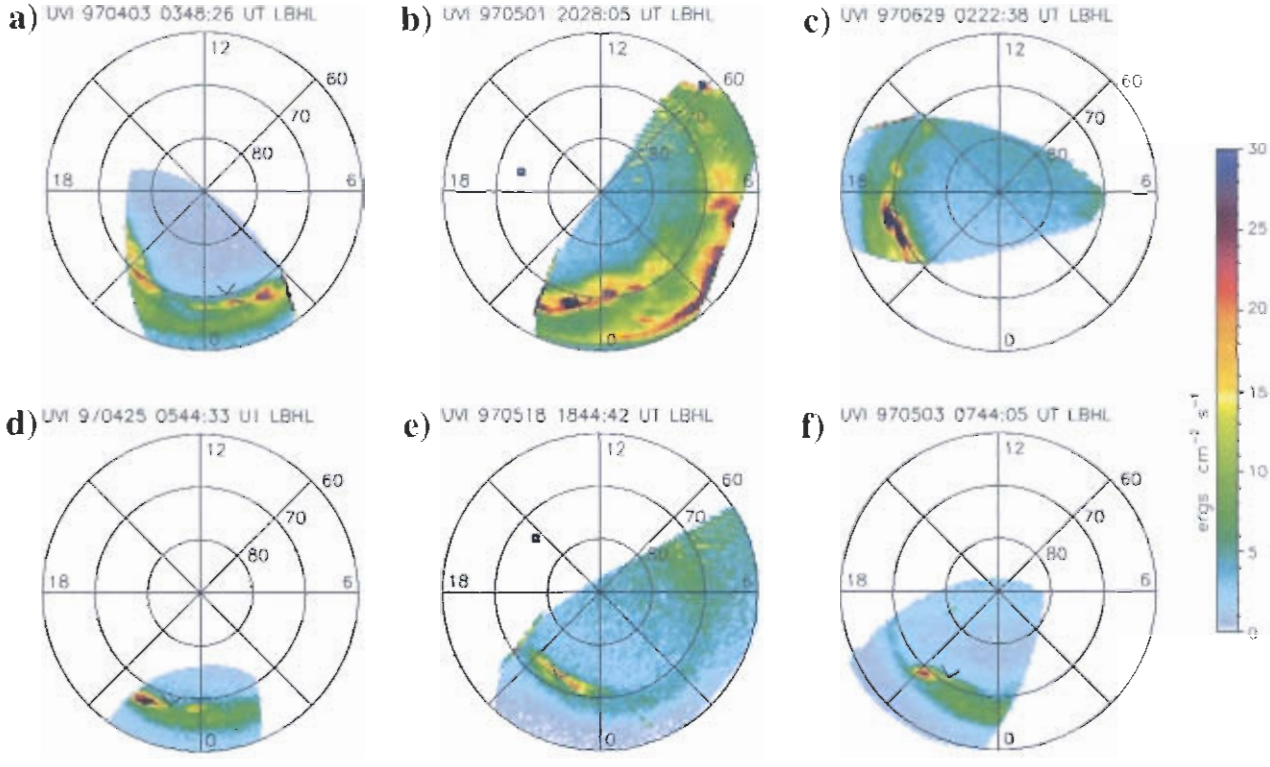

Poynting flux events smaller than 10 ergs $cm^{-2} s^{-1}$ (mapped)

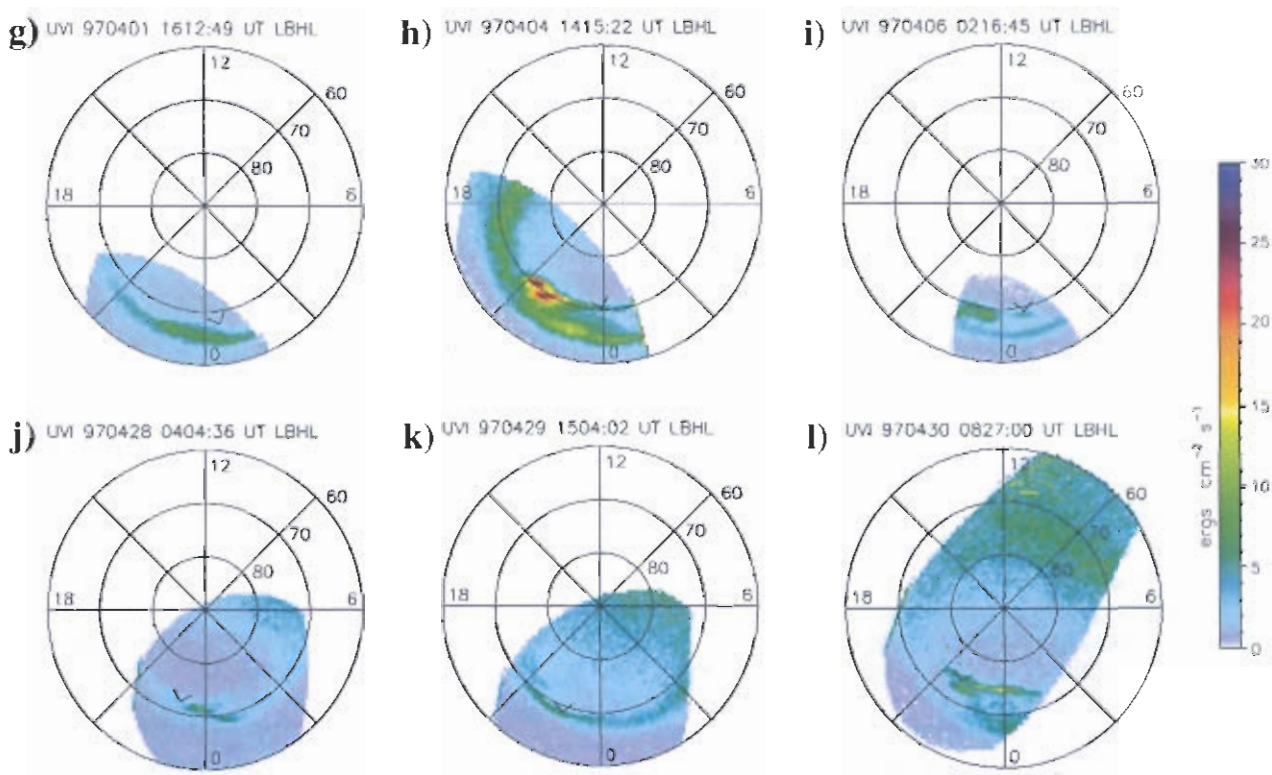

gradual increase in particle flux compared with the event on 21 April 1997. A region of small electric fields is observed for a period of ~25 min. Within this region the electric field reaches amplitudes of only 15 mV m^{-1} (6-s averaged). The electric field fluctuations also coincide with small magnetic field fluctuations. The E-to-B ratio and phasing suggest that these perturbations are of Alfvénic nature. Poynting flux calculations using the full 3-D electric and magnetic field vectors yield values less than 0.02 ergs cm^{-2} s^{-1} or less than 2.5 ergs cm^{-2} s^{-1} when mapped down to ionospheric altitudes. This is 2 orders of magnitude smaller compared with the event on 21 April 21 1997.

[22] The arrows in Figure 3 indicate the times of the sequence of the UVI images. In contrast to the event on 21 April 1997, the auroral arc was weak and had disappeared in the last image. The arc occurred at the higher invariant latitude of 72°. The mapped position of Polar's foot point moves southward across the auroral structure by ~1°. From Figures 3h to 3i, Polar entered the PSBL and encountered the turbulent region of small electric fields. In the vicinity of Polar's foot point during this time, the peak electron flux is between 2 and 4 ergs cm^{-2} s^{-1}. This is of the order of magnitude as the mapped in situ Poynting flux. Together with the previous event (21 April 1997), this suggests that the electromagnetic energy flow at high altitude is directly related to the energy flow at low altitude, which will be further supported in section 4.

[23] Ground magnetometer data show that the time period covered in the UVI images coincides with the recovery phase of a substorm (not shown). This is in agreement with other features of this event, which are a fading arc appearing at higher latitude (compared with the event on 21 April 1997) in a double-oval configuration and an expanded plasma sheet, inferred from the encounter of the poleward edge of the plasma sheet at higher L value (compared with the event on 21 April 1997). Furthermore, the plasma sheet particle signature is different compared with that of the event on 21 April 1997. There is not a sharp transition between the lobe and the PSBL, and the mean particle energy is less. The new result is that the electromagnetic energy flow in the PSBL at ~6 R_E is much reduced compared to a very active time (compare 21 April 1997).

4. Statistical Results

[24] A similar analysis to the previous two examples was done for a total of 40 plasma sheet crossings. The Polar events chosen for comparison come from a statistical study on large electric fields in the plasma sheet by *Keiling et al.* [2001]. In this study it was shown that the largest electric field events ($|E_\perp| \geq 100$ mV m^{-1}) were associated with large, downward, field-aligned Poynting flux (~1 ergs cm^{-2} s^{-1}). For eight events, simultaneous UV images were available and thus suitable for the comparison presented here. In addition, we searched the database for plasma sheet crossings that showed smaller Poynting flux values, and we compared those to UVI images as well. Geomagnetic activity for all 40 events ranged from quiet to very active.

4.1. Energy Flux Comparison

[25] After calculating the Poynting flux for all selected events as described in section 2, we recorded the largest value of Poynting flux at the satellite's location for each plasma sheet crossing. Next, UVI images taken at times closest to the Poynting flux observations were consulted. Because images are separated by ~2–3 min, the image that showed the larger emission, taken either immediately before or after the time of the Poynting flux event, was selected for comparison. Figure 4 shows 12 examples in addition to the previous two case studies (21 and 6 April 1997). Figures 4a–4f are examples of intense auroras, whereas Figures 4g–4l show weak auroras. Polar's foot point and its direction of motion are again marked as an arrow. Each panel corresponds to a different plasma sheet crossing by Polar. Poynting flux values ranged between 14 and 30 ergs cm^{-2} s^{-1} (mapped) for the intense auroras, whereas they were on the order of 5 ergs cm^{-2} s^{-1} (mapped) or less for weak auroras.

[26] The peak energy flux of auroral electrons, inferred from the UVI images, within 1° latitude and 0.5 hours MLT of the spacecraft foot point for all 40 conjugacies is plotted in Figure 5a versus the in situ peak Poynting flux. The error bars represent uncertainties of 50% associated with the estimates of electron energy flux [*Germany et al.*, 1998]. Error bars for only three events are shown because owing to the logarithmic scale, the error bars are of equal length for all events in this figure. Additional uncertainties with our method, which are not included in the error bars, arise from the fact that auroras vary on spatial and temporal scales smaller than the UVI images can resolve. There are also uncertainties with the mapping of the magnetic field line from Polar's location to altitudes of 100 km, which are of the order of degrees. Figure 5a shows clearly that the energy fluxes at low and high altitudes are correlated in the same way as was demonstrated for the two case studies earlier in this section: large (small) Poynting flux observed by Polar is associated with large (small) electron energy flux in the ionosphere.

[27] Figure 5a also shows that the in situ Poynting flux reached values up to ~2 ergs cm^{-2} s^{-1}. In order to determine whether the in situ Poynting flux is sufficient to provide the power for generating the magnetically conjugate, low-altitude electron energy flux, we mapped the in situ flux to ionospheric altitudes (~100 km). Because the geocentric distance and the ambient magnetic field strength were different for each event, we did not use a constant mapping factor but used (3) instead. The resulting distribution is shown in Figure 5b. The dashed line indicates the condition where mapped Poynting flux and electron energy flux are equal. The large majority of events lie above the line, which is consistent with the scenario where the high-altitude Poynting flux provides the power for the auroral electron beams. It is also interesting to note that the

Figure 4. (opposite) (a–l) Twelve representative events (out of 40) for which energy flux comparisons were done. Figures 4a–4f show auroras when Polar encountered conjugate Poynting flux events larger than 10 ergs cm^{-2} s^{-1} (when mapped to ~100-km altitude). Figures 4g–4l correspond to Poynting flux events smaller than 10 ergs cm^{-2} s^{-1} (mapped).

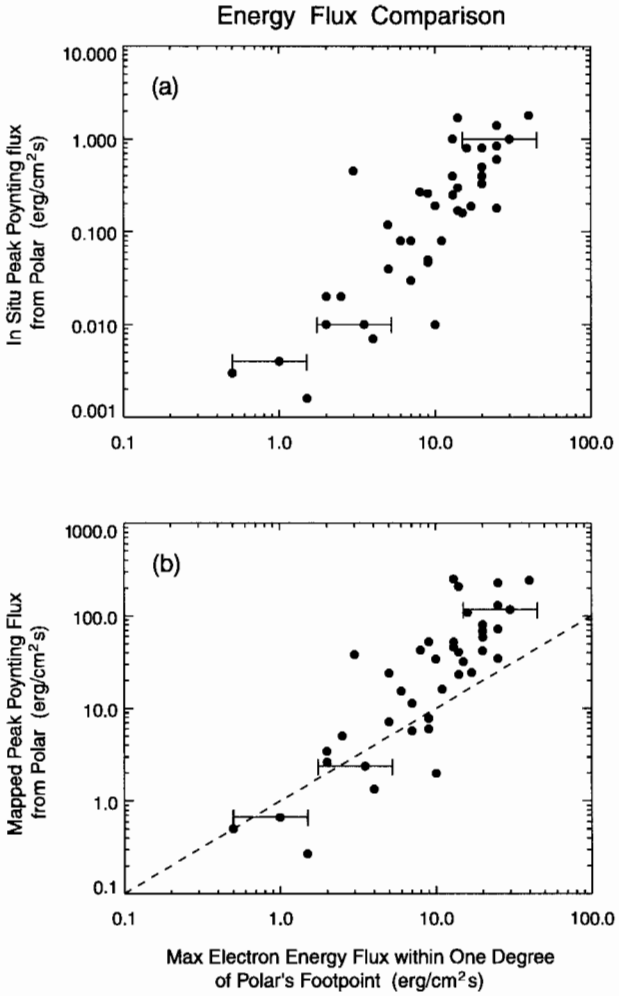

Figure 5. (a,b) Energy flux comparison for 40 events. In Figure 5a the scale on the y axis shows Poynting flux calculated from in situ electric and magnetic field measurements by Polar. The scale on the x axis shows the energy flux deposited into the ionosphere by electrons determined from UVI images (see text for description). The largest value within 1° of Polar's foot point at the time of the largest in situ Poynting flux is shown. Figure 5b is similar to Figure 5a, but the Poynting flux is mapped to altitudes of ~100-km using equation (3). The dashed line indicates the condition where mapped Poynting flux and electron energy flux are equal.

Poynting flux at the spacecraft location for the largest energy flow events is up to 10 times larger than that required to power the magnetically conjugate aurora. This allows for additional dissipation processes during times of active auroras such as ion acceleration, Joule heating, auroral kilometric radiation (AKR), etc., powered by the Poynting flux. It is also possible that the Poynting flux and the auroral electron beams at lower altitude broadened, which would reduce the energy flux compared with the high-altitude value. Note that the resolution of the UVI images does not allow one to discern individual arcs. The intensities shown in the UVI images are averaged over an entire pixel. Thus individual arcs could have somewhat higher intensities than those shown in the images.

[28] The more quiet events, on the other hand, lie closer to (and sometimes below) the dashed line. This is consistent with the fact that during quiet times, less additional energy for ion acceleration, Joule heating, etc., is needed. It is also possible that the events associated with weak auroras were cases of diffuse aurora rather than discrete aurora. The diffuse aurora is believed to be caused by direct precipitation of energetic plasma sheet particles. The high-altitude Poynting flux can thus be lower than that observed in the auroral emissions, because the electrons are not accelerated by energy conversion processes. In contrast, the large intensity of auroral emission during periods of strong Poynting flux suggests that these are cases of discrete aurora, which requires auroral acceleration processes, possibly powered by the magnetically conjugate Poynting flux observed at Polar's location. In any case, Figure 5 demonstrates a direct correlation of the intensity of Poynting flux with the intensity of ionospheric electron energy flux.

[29] With regard to the origin of the electromagnetic energy observed at Polar's location, we conclude on the basis of E-to-B ratio and phase relationship that the majority of events were of Alfvénic origin. For about one third of the events the ratios of the electric over the magnetic fields were in the range from 8000 to 15,000 km s^{-1}, which is comparable to the local Alfvén speeds (calculated from the local plasma density and the magnetic field strength) ranging from 10,000 to 20,000 km s^{-1} (100% H+) in the altitude range from 5 to 7 R_E [*Keiling et al.*, 2001]. In the case of quasi-static electric fields and field-aligned currents closing in the ionosphere, assuming no parallel potential drop, the E-to-B ratio is determined by $E_x = 1/(\mu_0 \Sigma_P) B_y$, where Σ_P is the height-integrated Pedersen conductivity and μ_0 is the magnetic permeability of free space [*Smiddy et al.*, 1980]. In an area of auroral electron precipitation, $\Sigma_P \sim 5$–10 mho, thus yielding $E_x/B_y = 80$–150 km s^{-1}, which is much lower than the observed E-to-B ratio, supporting the Alfvén wave interpretation. Although the remaining events had ratios less than 8000 km s^{-1} (but larger than 1000 km s^{-1}), their phase relationship was also often more complicated. In a static field scenario, however, E_x and B_y should be in phase as implied by the equation given above. Instead, the signals showed signatures of superposition of incident and reflected Alfvén waves. For electromagnetic waves the tangential electric fields of the incident and reflected waves subtract at a conducting surface such as the ionosphere, whereas those of the magnetic field add. Therefore the resulting signals can show complicated phase relationships once away from the reflection point. Additionally, because the ionosphere is not a perfectly reflecting surface and layers at higher altitude may also reflect Alfvén waves (such as the anomalous resistive layer [*Lysak and Dum*, 1983]), the phase relationship between E_x and B_x is further complicated. The wave periods of the field fluctuations for the events presented in this study vary from a few seconds to up to 1 min. Assuming that those observed periods are the actual periods, the wavelength, $\lambda_\parallel$, of the Alfvén waves varied from a few R_E to many tens of R_E, which is larger than the distance from Polar to the ionosphere. Thus, in cases where interference occurs, the E-to-B ratio should be intermediate between the ionospheric ratio and the Alfvénic ratio [*Mallinckrodt and Carlson*, 1978; *Lysak*,

1990]. The event on 21 April 1997 is an example without significant interference; E_x and B_y are mostly in phase, and the E-to-B ratio is Alfvénic. In cases where E_x and B_y are in perfect phase quadrature (90°), the E-to-B ratio is not an appropriate indicator for Alfvén waves at all, because this ratio largely depends on how close to an electric or magnetic field node the field measurements were made. In this case one can, however, completely rely on the phase lag of 90°,which can only exist for an electromagnetic wave and not for static fields. Alfvén waves with local standing wave structure are also present in our database. Their properties will be further investigated in a future paper.

4.2. Mapping the Aurora

[30] In addition to the energy flux comparison, one additional observation can be made. The large Poynting flux events recorded in the PSBL mapped to the poleward border of the active auroral region. Note that large Poynting flux events were also recorded further into the central plasma sheet (CPS), but because the UVI turns off at lower altitudes, no simultaneous images were available for these events. No widely accepted picture exists regarding the mapping of auroral features into the magnetotail (see review by *Elphinstone et al.* [1993]). Our observations provide additional evidence that the poleward border of the auroral oval maps to the PSBL. The mappingwas done with the IGRF model. Since the Poynting flux events reported herein are within 7 R_E, i.e., within the region of the dipole-like Earth's magnetic field, we estimate its accuracy to be on the order of degrees. In 90% of the events included in our statistics, Polar was on an inbound pass crossing the lobe-PSBL interface from the tail lobe. The largest Poynting flux was recorded at or near the interface. The identification of the PSBL was facilitated by the fact that all but one event coincided with the first encounter of the plasma sheet, which leaves little doubt about its identification. This result combined with the fact that Polar's foot point was located at or near the poleward border of the auroral region strongly supports the view that the PSBL maps to the poleward region of the aurora.

5. Summary and Discussion

[31] We have investigated the energy flux of auroral electrons into the ionosphere (inferred from UVI images) during 40 Polar encounters with the plasma sheet with a range of Poynting flux values to establish a correlation between high-altitude and low-altitude energy flows. The results are summarized as follows:

1. The magnitudes of Poynting flux measured in the plasma sheet (4–7 R_E) were correlated to ionospheric electron energy flux (or equivalently auroral emission) in magnetically conjugate regions. Large in situ Poynting flux was magnetically conjugate to intense auroral emissions, whereas small Poynting flux was magnetically conjugate to weak or no auroral emission.

2. The majority of the events could be identified as Alfvén waves on the basis of E-to-B ratios and phase relationships; a few events ($\leq$30%) remain uncertain.

3. The largest Poynting flux events exceeded 1 ergs cm^{-2} s^{-1}, the largest being 2 ergs cm^{-2} s^{-1}. When mapped to the ionosphere, assuming conservation of Poynting flux, these values correspond to 125 and 300 ergs cm^{-2} s^{-1}, respectively. This Poynting flux was predominantly downward and was large enough to account for the conjugate electron energy flux at altitudes of ~100 km.

4. The mapped Poynting flux obtained by Polar was 1–10 times larger than the energy flux inferred from UVI images at low altitude. If the Poynting flux is indeed responsible for energizing the auroral electrons, then up to 10 times larger Poynting flux could also provide the energy for additional energy dissipation processes such as Joule heating, ion acceleration, etc.

5. The large Poynting fluxes were generally found near the outer boundary of the plasma sheet, i.e., the PSBL. This location mapped to the poleward border of simultaneous auroral emissions. This suggests that the aurora near the polar cap boundary is associated with Alfvén wave energy.

[32] This is the first statistical study to correlate auroral emissions (or equivalently, electron precipitation) in the ionosphere with Poynting flux in the plasma sheet. The results provide evidence for a link of a magnetospheric energy transfer process in the magnetotail and auroral luminosity. For the majority of the events we confirmed that the intense, localized high-altitude energy flux was due to Alfvén waves. It is interesting to note that the magnitude of the Poynting flux observed with other satellites and rockets [*Kelley et al.*, 1991; *Louarn et al.*, 1994; *Nagatsuma et al.*, 1996; *Kletzing et al.*, 1996] at low altitudes is smaller than Polar's mapped Poynting flux, supporting the scenario where the high-altitude Poynting flux is dissipated in the acceleration of electrons. For example, *Nagatsuma et al.* [1996], using the Akebono satellite, reported Alfvén waves at altitudes below 8000 km with equal amplitudes of incident and reflected waves. The reported Poynting flux (up to 4 ergs cm^{-2} s^{-1}) was much smaller than our Polar observations. Hence, together with our observation of mostly downward Poynting flux, it suggests that the high-altitude Poynting flux is indeed dissipated through particle acceleration within the auroral acceleration region.

[33] The larger Poynting flux events observed by Polar were confined to a thin spatial layer ($\leq$0.5° invariant latitude in the spacecraft frame) in comparison to the entire plasma sheet. Because of the relative velocities between Polar (1–2 km s^{-1}) and the plasma sheet, which can expand at larger velocities, the latitudinal extent of this layer can be larger. On the other hand, the scale size of the entire region of auroral emission for the events investigated was $\leq$6° in latitude. Hence it is not clear whether the high-altitude Poynting flux supplies enough energy for the entire auroral region or only for the immediate vicinity of the magnetically conjugate region. It is also not possible from our study to determine whether the Poynting flux layer broadened at lower altitude. This would require suitable conjunctions with low-altitude satellites. Similarly, it cannot be shown with one satellite whether the Poynting flux due to the Alfvén waves actually powered the conjugate aurora, although we clearly demonstrated that when there was strong Poynting flux at Polar's location, auroral emission was strong, and, furthermore, the Poynting flux was sufficient to account for the magnetically conjugate, ionospheric electron energy flux causing the emission. The intense aurora events, included in this study, were most likely cases of discrete auroras, which involve acceleration processes at

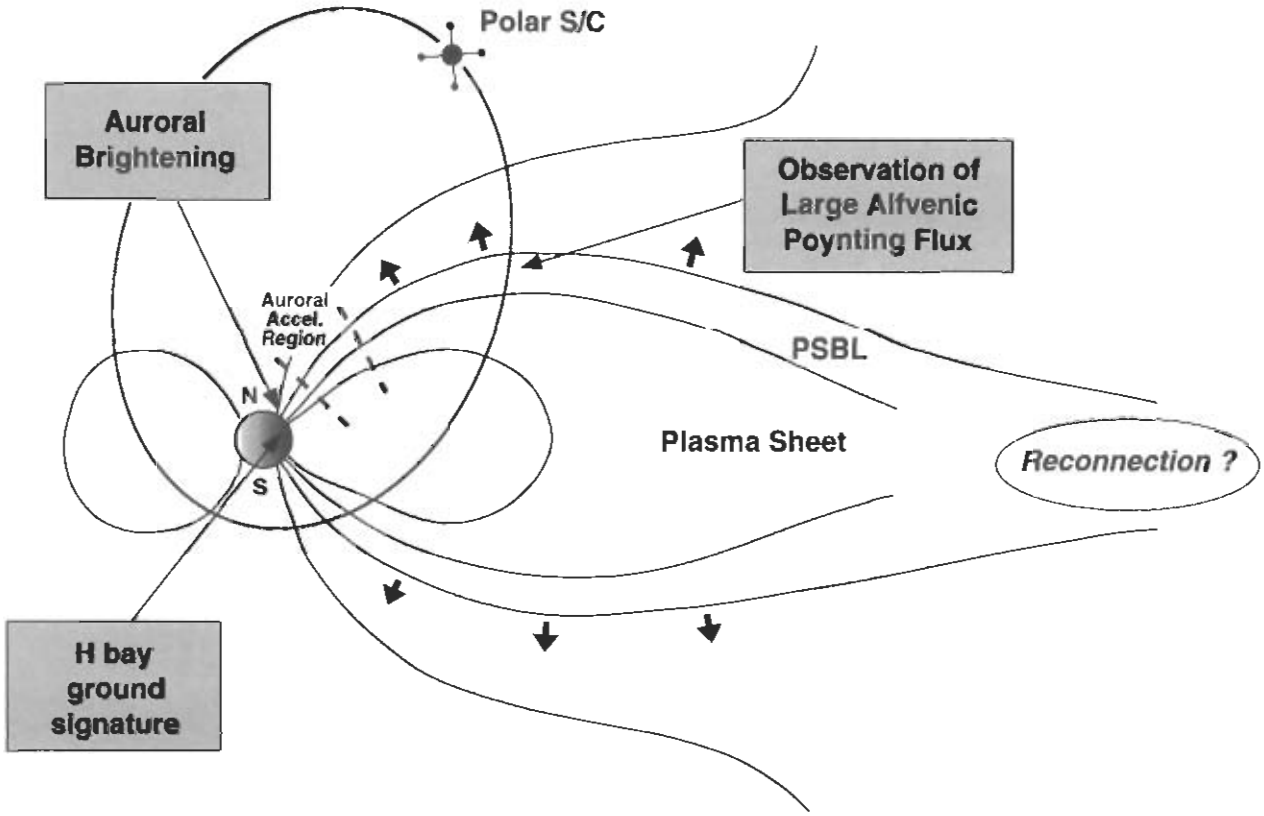

Figure 6. Cartoon showing the connection of auroral phenomena, such as auroral brightening, negative H bay, and large Alfvén waves in the plasma sheet boundary layer (PSBL). Alfvén waves, possibly generated at the reconnection site, propagate toward the ionosphere along magnetic field lines. Electrons accelerated by the Alfvén waves precipitate into the ionosphere, causing auroral brightening. Simultaneously, ground magnetometer data show magnetic bays.

lower altitude, possibly powered by the large Alfvén waves. The weak aurora events associated with small plasma sheet Poynting flux, on the other hand, were possibly cases of diffuse aurora, which is believed to be mainly caused by direct precipitation of very energetic plasma sheet particles.

[34] The causal connection between Alfvén waves and auroral emissions is supported by theoretical studies that provide models for auroral arc formation due to Alfvén waves. It is suggested that shear Alfvén waves become in the small-scale limit, kinetic Alfvén waves at steep density gradients [e.g., *Hasegawa*, 1976; *Goertz and Boswell*, 1979; *Lysak and Lotko*, 1996]. Kinetic Alfvén waves can accelerate electrons via parallel electric fields. There is observational evidence for kinetic Alfvén waves in association with several of the events included in this study [*Wygant et al.*, 2001] as well as at lower altitudes [e.g., *Louarn et al.*, 1994]. Furthermore, an anomalously resistive layer has been considered as a region that can sustain a parallel electric field and thus lead to particle acceleration [*Lysak and Dum*, 1983; *Lotko et al.*, 1998; *Streltsov and Lotko*, 1999]. In an unpublished manuscript by A.V. Streltsov et al. (2001), numerical modeling of the 21 April 1997 event (described in section 3) shows that its electromagnetic signature could be reproduced by assuming a shear Alfvén wave model, and the inclusion of anomalous resistivity in the model led to parallel electric fields large enough to account for significant parallel electron acceleration.

[35] Many processes in the magnetosphere are linked to the auroral oval, resulting in intense particle precipitation and auroral emissions. There is, however, still disagreement as to where auroral arcs map from in the magnetosphere. The inner edge has been associated with the break-up arc [*Samson et al.*, 1991], and large Poynting flux has been observed at the inner edge of the plasma sheet [*Maynard et al.*, 1996]. Large Poynting flux was also observed inside the CPS [*Keiling et al.*, 2001; *Toivanen et al.*, 2001]. Some studies regard the boundary plasma sheet (BPS) as the key region for auroral arcs. On the basis of our statistical study, we can conclude that the PSBL plays a key role. All events for which we recorded large Poynting flux values in the PSBL mapped to the poleward border of active auroral regions in the ionosphere. It was not possible to compare Poynting flux measurements to UVI images when Polar was further into the CPS, because at lower latitudes the imager is turned off.

[36] In identifying the different processes for the transport of energy in the magneto tail, it is now known that both plasma transport and electromagnetic energy in the form of field-aligned currents (FACs) and Alfvén waves carry large amounts of energy earthward in association with substorms. Quasi-static FACs are closely associated with auroral phenomena and energy transport. The Birkeland current system maps into the auroral oval [*Iijima and Potemra*, 1976], transmitting power from the tail to the ionosphere. During

substorms, additional FACs form, which enhance the energy transfer. Discrete bursts of high-velocity plasma flow in the equatorial plane (BBF) carry considerable energy earthwards [*Angelopoulos et al.*, 1992; *Fairfield et al.*, 1999]. For some events it was shown that they occur in close temporal and magnetic conjugacy to auroral brightening [*Fairfield et al.*, 1999]. On the other hand, the study by *Wygant et al.* [2000] and the study presented herein show that large Alfvénic Poynting flux at high altitudes is also magnetically conjugate to intense auroral emissions, which shows the importance of Alfvén waves as a means of energy transport from the distant magnetotail to the acceleration region. Further, it supports the view that Alfvén waves contribute to the arc generation process. Including the works of *Keiling et al.* [2000] and *Toivanen et al.* [2001], showing large Poynting flux during the substorm expansion phase, Figure 6 illustrates the connection of auroral penomena, such as auroral brightening, negative H bay, and Alfvén wave energy flow in the PSBL. Although we have shown that the Alfvénic energy flux is sufficient to account for magnetically conjugate, low-altitude auroral phenomena, it is important to investigate whether BBF and Alfvén waves occur simultaneously, and if so, whether they are generated from the same process in the magnetotail and which one is the dominant energy transport mechanism.

[37] Finally, we have not attempted to separate our observations according to different schemes, such as substorms [*Akasofu*, 1964], pseudo breakup [*Koskinen et al.*, 1993], and poleward boundary intensifications [*Lyons et al.*, 1999]. This would be a worthwhile extension of this work.

[38] **Acknowledgments.** Analysis of electric field data was supported by NASA International Solar Terrestrial Program (NASA contract NAG 5-3182). Analysis of magnetometer data was supported by NASA NAG 5-7721. Work at the University of Iowa in analysis of Hydra data was performed under NASA grant 5-2231 and DARA grant 50 OC 8911 0. Work at the University of Washington was supported by NASA grant NAG 5-3170. We thank the referees for their comments. One of the authors (A. K.) thanks R. Lysak and Y. Song for helpful discussions.

[39] Hiroshi Matsumoto thanks the referees for their assistance in evaluating this paper.

References

Akasofu, S.-I., The development of the auroral substorm, *Planet. Space Sci.*, *12*, 273–282, 1964.

Angelopoulos, V., W. Baumjohann, C. F. Kennel, F. V. Coroniti, M. G. Kivelson, R. Pellat, R. J. Walker, H. Luhr, and G. Paschmann, Bursty bulk flows in the inner central plasma sheet, *J. Geophys. Res.*, *97*, 4027–4039, 1992.

Baker, D. N., T. I. Pulkkinen, V. Angelopoulos, W. Baumjohann, and R. L. McPherron, Neutral line model of substorms: Past results and present view, *J. Geophys. Res.*, *101*, 12,975–13,010, 1996.

Bennett, E. L., M. Temerin, and F. S. Mozer, The distribution of auroral electrostatic shocks below 8000-km altitude, *J. Geophys. Res.*, *88*, 7107–7120, 1983.

Cattell, C. A., M. Kim, R. P. Lin, and F. S. Mozer, Observations of large electric fields near the plasma sheet boundary by ISEE-1, *Geophys. Res. Lett.*, *9*, 539–542, 1982.

Cattell, C. A., F. S. Mozer, K. Tsuruda, H. Hayakawa, M. Nakamura, T. Okada, S. Kokubun, and T. Yamamoto, Geotail observations of spiky electric fields and low-frequency waves in the plasma sheet and plasma sheet boundary, *Geophys. Res. Lett.*, *21*, 2987–2990, 1994.

Elphinstone, R. D., et al., The auroral distribution and its mapping according to substorm phase, *J. Atmos. Terr. Phys.*, *55*, 1741–1762, 1993.

Fairfield, D. H., et al., Earthward flow bursts in the inner magnetotail and their relation to auroral brightenings, AKR intensifications, geosynchronous particle injections and magnetic activity, *J. Geophys. Res.*, *104*, 355–370, 1999.

Germany, G. A., J. F. Spann, G. K. Parks, M. J. Brittnacher, R. Elsen, L. Chen, D. Lummerzheim, and M. H. Rees, Auroral observations from the Polar Ultraviolet Imager (UVI), in *Geospace Mass and Energy Flow: Results From the International Solar-Terrestrial Physics Program*, *Geophys. Monogr. Ser.*, vol. 104, edited by J. L. Horwitz, D. L. Gallagher, and W. K. Peterson, pp. 149–160, AGU, Washington, D.C., 1998.

Goertz, C. K., Kinetic Alfvén waves on auroral field lines, *Planet. Space Sci.*, *32*, 1387–1392, 1984.

Goertz, C. K., and R. W. Boswell, Magnetosphere-ionosphere coupling, *J. Geophys. Res.*, *84*, 7239–7246, 1979.

Harvey, P., et al., The electric field instrument on the Polar satellite, in *The Global Geospace Mission*, edited by C. T. Russell, pp. 583–596, Kluwer Acad., Norwell, Mass., 1995.

Hasegawa, A., Particle acceleration by MHD surface wave and formation of aurora, *J. Geophys. Res.*, *81*, 5083–5090, 1976.

Iijima, T., and T. A. Potemra, The amplitude distribution of field-aligned currents at northern high latitudes observed by Triad, *J. Geophys. Res.*, *81*, 2165–2174, 1976.

Keiling, A., J. R. Wygant, C. A. Cattell, M. Temerin, F. S. Mozer, C. A. Kletzing, J. D. Scudder, C. T. Russell, W. Lotko, and A. V. Streltsov, Large Alfvén wave power in the plasma sheet boundary layer during the expansion phase of substorms, *Geophys. Res. Lett.*, *27*, 3169–3173, 2000.

Keiling, A., J. R. Wygant, C. A. Cattell, M. Johnson, M. Temerin, F. S. Mozer, C. A. Kletzing, J. Scudder, and C. T. Russell, Properties of large electric fields in the plasma sheet at 4–7 R_E measured with Polar, *J. Geophys. Res.*, *106*, 5779–5798, 2001.

Kelley, M. C., D. J. Knudsen, and J. F. Vickery, Poynting flux measurements on a satellite: A diagnostic tool for space research, *J. Geophys. Res.*, *96*, 201–207, 1991.

Kletzing, C. A., C. Cattell, F. S. Mozer, S.-I. Akasofu, and K. Makita, Evidence for electrostatic shocks as the source of discrete auroral arcs, *J. Geophys. Res.*, *88*, 4105–4113, 1983.

Kletzing, C. A., et al., The electrical and precipitation characteristics of morning sector Sun-aligned auroral arcs, *J. Geophys. Res.*, *101*, 17,175–17,189, 1996.

Koskinen, H. E. J., R. E. Lopez, R. J. Pellinen, T. I. Pulkinen, and D. N. Baker, Pseudo-breakups and substorm growth phase in the ionosphere and magnetosphere, *J. Geophys. Res.*, *98*, 5801–5813, 1993.

Levin, S., K. Whitley, and F. S. Mozer, A statistical study of large electric field events in the Earth's magnetotail, *J. Geophys. Res.*, *88*, 7765–7768, 1983.

Liu, W. W., B.-L. Xu, J. C. Samson, and G. Rostoker, Theory and observation of auroral substorms: A magnetohydrodynamic approach, *J. Geophys. Res.*, *100*, 79–95, 1995.

Lotko, W., A. V. Streltsov, and C. W. Carlson, Discrete auroral arc, electrostatic shock and suprathermal electrons powered by dispersive, anomalously resistive field line resonance, *Geophys. Res. Lett.*, *25*, 4449–4452, 1998.

Louarn, P., J.-E. Wahlund, T. Chust, H. de Feraudy, A. Roux, B. Holback, P. O. Dovner, A. I. Eriksson, and G. Holmgren, Observations of kinetic Alfvén waves by the Freja satellite, *Geophys. Res. Lett.*, *21*, 195–205, 1994.

Lyons, L. R., et al., Association between Geotail plasma flows and auroral poleward boundary intensifications observed by CANOPUS photometers, *J. Geophys. Res.*, *104*, 4485–4500, 1999.

Lysak, R. L., Electrodynamic coupling of the magnetosphere and ionosphere, *Space Sci. Rev.*, *52*, 33–87, 1990.

Lysak, R. L., and C. T. Dum, Dynamics of magnetosphere-ionosphere coupling including turbulent transport, *J. Geophys. Res.*, *88*, 365–380, 1983.

Lysak, R. L., and W. Lotko, On the dispersion relation for shear Alfvén waves, *J. Geophys. Res.*, *101*, 5085–5094, 1996.

Mallinckrodt, A. J., and C. W. Carlson, Relations between transverse electric field sand field-aligned currents, *J. Geophys. Res.*, *83*, 1426–1432, 1978.

Maynard, N. C., W. J. Burke, E. M. Basinska, G. M. Erickson, W. J. Hughes, H. J. Singer, A. G. Yahnin, D. A. Hardy, and F. S. Mozer, Dynamics of the inner magnetosphere near times of substorm onset, *J. Geophys. Res.*, *101*, 7705–7736, 1996.

McIlwain, C. E., Direct measurements of particle producing visible aurorae, *J. Geophys. Res.*, *65*, 2727–2747, 1960.

Mozer, F. S., et al., Observations of paired electrostatic shocks in the polar magnetosphere, *Phys. Rev. Lett.*, *38*, 292–295, 1977.

Mozer, F. S., ISEE-1 observations of electrostatic shocks on auroral zone field lines between 2.5 and 7 Earth radii, *Geophys. Res. Lett.*, *8*, 823–826, 1981.

Nagatsuma, T., et al., Field-aligned currents associated with Alfvén waves in the poleward boundary region of the nightside auroral oval, *J. Geophys. Res.*, *101*, 21,715–21,730, 1996.

Russell, C. T., R. C. Snare, J. D. Means, D. Pierce, D. Dearborn, M. Larson, G. Barr, and G. Le, The GGS/Polar Magnetic Fields Investigation, in *The Global Geospace Mission*, edited by C. T. Russell, pp. 563–582, Kluwer Acad., Norwell, Mass., 1995.

Samson, J. C., T. J. Hughes, F. Creutzberg, D. D. Wallis, R. A. Greenwald, and J. M. Ruohoniemi, Observations of a detached, discrete arc in association with field line resonances, *J. Geophys. Res.*, *96*, 15,683–15,695, 1991.

Samson, J. C., L. L. Cogger, and Q. Pao, Observations of field line resonances, auroral arcs, and auroral vortex structures, *J. Geophys. Res.*, *101*, 17,373–17,383, 1996.

Scudder, J., et al., Hydra: A 3-dimensional electron and ion hot plasma instrument for the Polar spacecraft of the GGS mission, in *The Global Geospace Mission*, edited by C. T. Russell, pp. 459–495, Kluwer Acad., Norwell, Mass., 1995.

Smiddy, M., W. J. Burke, M. C. Kelley, N. A. Saflekos, M. S. Gussenhoven, D. A. Hardy, and F. J. Rich, Effects of high-latitude conductivity on observed convection electric fields and Birkeland currents, *J. Geophys. Res.*, *85*, 6811–6818, 1980.

Streed, T., C. Cattell, F. Mozer, S. Kokubun, and K. Tsuruda, Spiky electric fields in the magnetotail, *J. Geophys. Res.*, *106*, 6275–6289, 2001.

Streltsov, A. V., and W. Lotko, Dispersive, nonradiative field line resonances in a dipolar magnetic field geometry, *J. Geophys. Res.*, *102*, 27,121–27,135, 1997.

Streltsov, A. V., and W. Lotko, Small-scale, "electrostatic" auroral structures and Alfvén waves, *J. Geophys. Res.*, *104*, 4411–4426, 1999.

Toivanen, P. K., D. N. Baker, W. K. Peterson, X. Li, E. F. Donovan, A. Viljanen, A. Keiling, and J. R. Wygant, Plasma sheet dynamics observed by the Polar spacecraft in association with substorm onsets, *J. Geophys. Res.*, *106*, 19,117–19,130, 2001.

Torbert, R. B., and F. S. Mozer, Electrostatic shocks as the source of discrete auroral arcs, *Geophys. Res. Lett.*, *5*, 135–138, 1978.

Torr, M. R., et al., A far ultraviolet imager for the International Solar-Terrestrial Physics Mission, in *The Global Geospace Mission*, edited by C. T. Russell, pp. 459–495, Kluwer Acad., Norwell, Mass., 1995.

Wahlund, J.-E., P. Louarn, T. Chust, H. de Feraudy, A. Roux, B. Holback, P.-O. Dovner, and G. Holmgren, On ion acoustic turbulence and the nonlinear evolution of kinetic Alfvén waves in Aurora, *Geophys. Res. Lett.*, *21*, 1831–1834, 1994.

Wygant, J. R., et al., Polar spacecraft based comparisons of intense electric fields and Poynting flux near and within the plasma sheet–tail lobe boundary to UVI images: An energy source for the Aurora, *J. Geophys. Res.*, *105*, 18,675–18,692, 2000.

Wygant, J. R., A. Keiling, C. A. Cattell, R. L. Lysak, M. Temerin, F. S. Mozer, C. A. Kletzing, J. D. Scudder, W. Peterson, and C. T. Russell, Evidence for kinetic Alfvén waves and parallel electron energization at 5–7 R_E altitudes in the plasma sheet boundary layer, *J. Geophys. Res.*, in press, 2002.

C. Cattell, A. Keiling, and J. R. Wygant, School of Physics and Astronomy, University of Minnesota, 116 Church Street SE, Minneapolis, MN 55455, USA. (akeiling@ham.space.umn.edu)

C. A. Kletzing, Department of Physics and Astronomy, University of Iowa, IA 52242, USA.

F. S. Mozer and M. Temerin, Space Sciences Laboratory, University of California, Berkeley, CA 94720, USA.

G. Parks and W. Peria, Geophysics Program, University of Washington, Seattle, WA 98195, USA.

C. T. Russell, IGPP, University of California, Los Angeles, CA 90095, USA.